Available online at www.sciencedirect.com

ScienceDirect

journal homepage: www.elsevier.com/locate/he

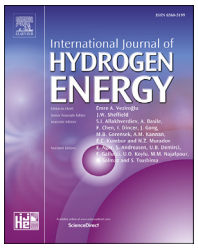

Parallel plates reactor simulation: Ethanol steam reforming thermally coupled with ethanol combustion

Eduardo M. Izurieta[*], *Daniel O. Borio*, *Marisa N. Pedernera*, *Eduardo López*

PLAPIQUI, Universidad Nacional del Sur (UNS) - CONICET, Bahía Blanca, Argentina

ARTICLE INFO

Article history:
Received 21 February 2017
Received in revised form
15 June 2017
Accepted 16 June 2017
Available online 8 July 2017

Keywords:
Ethanol steam reforming
Parallel plates reactor
Thermal coupling
Hydrogen production

ABSTRACT

This work presents a theoretical study on the thermal coupling of ethanol steam reforming with ethanol combustion in a parallel plates reactor. A one-dimensional, heterogeneous, mathematical model is used and the effects of the main operative and constructive variables on the performance of the system are analyzed. Thermal coupling between combustion and reforming of ethanol is plausible and an adequate behavior of the reactor in terms of hydrogen yield and conversion of ethanol is predicted. The importance of distributing the source of heat is evidenced since high molar fractions of ethanol in the combustion stream can lead to excessive hot spots.

© 2017 Hydrogen Energy Publications LLC. Published by Elsevier Ltd. All rights reserved.

Introduction

For decades, the rational use of renewable energy has been promoted to help solve the problems of power availability, environmental protection and regional development. In this context, hydrogen is presented as an interesting alternative, particularly when it proceeds from raw materials of biological origin [1]. Hydrogen is thought to be an energetic vector useful for power generation with fuel cells [2], but it is relatively difficult to store both in gas and liquid state, especially for mobile applications, turning it in a technical bottleneck in the development of this kind of systems [3]. Instead, the storage of a liquid fuel is proposed to generate hydrogen directly in the consumption location, avoiding expensive transportation and taking advantage from the compatibility with any current infrastructure of fuel supply. In this scenario, bioethanol from agricultural waste is a promising raw material since it presents low toxicity and easy storage, it possesses high energetic density [4] and can be obtained in an industrial mature process from the fermentation of cereals, sugar cane or beetroot [5,6]. Furthermore, ethanol processing produces approximately as much CO_2 as that consumed by biomass growth, conforming a closed carbon cycle [7] and therefore mitigating net carbon dioxide emissions.

Even though the stoichiometry of the reaction of ethanol steam reforming presents a maximum of 6 mol of hydrogen per mol of ethanol ($C_2H_5OH + H_2O \rightarrow 2CO_2 + 6H_2$), the system of reactions is complex and many pathways could be involved in the generation of the final products; the main and most commonly found final gaseous products being H_2, CO_2, CO and

* *Corresponding author*. PLAPIQUI, Universidad Nacional del Sur (UNS) - CONICET, Camino La Carrindanga km 7, 8000, Bahía Blanca, Argentina
E-mail address: eizurieta@plapiqui.edu.ar (E.M. Izurieta).

http://dx.doi.org/10.1016/j.ijhydene.2017.06.134
0360-3199/© 2017 Hydrogen Energy Publications LLC. Published by Elsevier Ltd. All rights reserved.

CH_4. It has been observed that these routes include the formation of different intermediaries as ethylene and/or acetaldehyde, among others [8,9], which can be principally found at short contact times and/or low temperatures, depending on the catalyst at hand [10]. Many of the involved reactions are equilibrium-limited [11], and this fact adds a strong constraint to the maximum hydrogen which can be produced at each operative condition.

Ethanol steam reforming is pointed as an ideal reaction to obtain hydrogen from ethanol based on the reaction stoichiometry, but as a counterpart, it presents a high endothermic character. Alternatively, literature [12,13], presents studies concerning steam reforming combined with partial oxidation to ensure autothermal operation but this approach leads to a clear diminishment in the maximum hydrogen yield that could be reached. Hence, the reformer must be carefully designed in terms of improving the heat transfer conditions from an external heat source to the reaction medium. Therefore, a practical implementation of this process requires extremely efficient reactors, capable of transferring elevated heat fluxes per unit area. To achieve these ends, parallel plates reactors (PPR) considering thermally coupled catalytic reactions of ethanol steam reforming (ESR) and ethanol combustion (EC) has been proposed in literature [14]. This kind of reactor is based on the idea of alternated channels, each one carrying out either the endothermic or the exothermic reaction, divided by metallic separators through which heat is transferred. Each channel of the unit is filled with a structured catalyst. Structured catalysts are selected based on the possibility of operation with low pressure drops and easier scaling up (numbering up) [15,16].

In the last decades, the interest in coupling endothermic and exothermic reactions has increased [17] due to the need of developing intensified processes. Frauhammer et al. [14] studied the coupling of methane steam reforming and methane combustion in a ceramic monolithic reactor, under a countercurrent configuration, finding that the heat released in the combustion reaction can be efficiently transferred to the reforming side even at low temperature gradients through both sides. The major problems of this type of units are the different reaction rates and heats of reaction in both sides, leading to an overheated zone inside the channels. As Kolios et al. [18,19], exposed in their research, this issue can be solved by adding distributed inlets of fuel and selecting a cocurrent configuration to diminish the heat generation rate along the reactor. Zanfir and Gavriilidis [20,21], concluded that hot spots could be avoided matching the ratio of heat generation to heat consumption by means of adjusting the load of catalyst, but they warned about other possible phenomena which should be studied, such as catalyst deactivation, which could lead to heat imbalances, or homogeneous reactions, which could be possible at high reactor temperatures.

The feasibility of this technology for ethanol steam reforming in structured reactors was previously studied experimentally by López et al. [22], using hydrogen combustion to provide the heat required in the process side. A satisfactory performance of the unit was measured in terms of thermal coupling and hydrogen production. Casanovas et al. [23] designed, modeled, and tested the generation of hydrogen from ethanol under autothermal regime coupling both steam reforming and combustion of ethanol in a structured microreactor proving good performance of the thermal coupling. The authors reported lower hot spots in the case of cocurrent configuration. Bruschi et al. reported theoretical studies regarding ethanol steam reforming in a metallic microreactor, coupled with flue gas from an external combustion chamber [24] or with ethanol combustion [25], showing the importance of the inlet temperature of the streams in order to achieve satisfactory results and the necessity of avoiding excessive hot spots inside the channels.

This work presents the analysis of a parallel plates reactor for hydrogen production from ethanol. The study is performed by using a mathematical model to optimize the design of a highly-efficient reaction unit, capable of operating under autothermal conditions. Focus is given here on the influence of operating variables as temperature and the concentration of ethanol fuel, and constructive variables as the distribution of ethanol fuel at different axial locations of the unit. The hydrogen yield, products selectivity, occurrence and position of hot spots and heat of reaction involved are followed to analyze the reactor performance.

Theoretical framework

Geometry of the parallel plates reactor

As mentioned before, the reactor (PPR) includes ethanol steam reforming coupled with ethanol combustion with air. These reactions are thought to be performed over a commercial catalyst deposited on ceramic (cordierite) monolithic structures washcoated with Pd/γ-Al_2O_3. A scheme of the reactor is presented in Fig. 1.

Each structure is separated from the neighbor by a metallic wall of stainless steel. While the blue sections of Fig. 1 represent the reforming sections of the reactor, the red ones are those corresponding to the combustion sections. L_Z, L_X and L_W are the reactor length, the thickness of the metallic wall and the width of the monoliths channels (square channels here), respectively. A design with 2 rows of channels per reactor section seems to be a reasonable compromise between

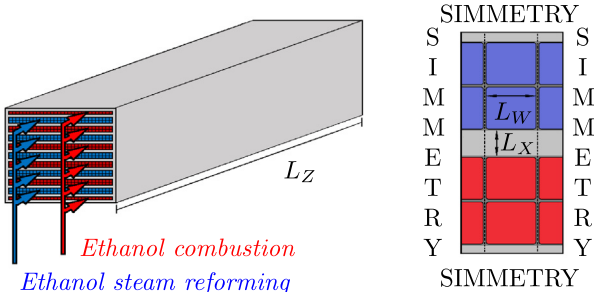

Fig. 1 – Left: Scheme of the parallel plates reactor with reforming (blue) and combustion (red) sections containing monolithic catalysts. Right: modeled domain as representative of the whole reactor. (For interpretation of the references to colour in this figure legend, the reader is referred to the web version of this article.)

mechanical stability of the ceramic monolith and adequate conditions for heat transfer between both catalyst zones.

Description of the system of reactions

The system of reactions representing the steam reforming strongly depends on the selected catalyst and several intermediaries can be obtained in different operative conditions [8]. In this case, it was considered appropriate to model the reaction scheme as follows, as it was reported by López et al. [22]:

$$C_2H_5OH + H_2O \rightarrow CH_4 + CO_2 + 2H_2 \quad \Delta H^o = 8.3\ kJ/mol \tag{1}$$

$$CH_4 + H_2O \leftrightarrow CO + 3H_2 \quad \Delta H^o = 206.1\ kJ/mol \tag{2}$$

$$CO + H_2O \leftrightarrow CO_2 + H_2 \quad \Delta H^o = -41.2\ kJ/mol \tag{3}$$

On the other hand, ethanol combustion is globally represented as a two-step reaction [25–27], presenting acetaldehyde as an intermediary:

$$C_2H_5OH + 1/2O_2 \rightarrow C_2H_4O + H_2O \quad \Delta H^o = -173.4\ kJ/mol \tag{4}$$

$$C_2H_4O + 5/2O_2 \rightarrow 2CO_2 + 2H_2O \quad \Delta H^o = -1104.3\ kJ/mol \tag{5}$$

Mathematical model

A one-dimensional heterogeneous model is selected to represent the parallel plates reactor. Steady state operation is assumed along with the following considerations:

- Isobaric operation: a low pressure drop can be assumed as the reactor sections are filled with monolithic catalysts with 1 mm^2 square channels.
- Thermally isolated reactor: heat loss to the environment is considered negligible due to the implementation of appropriate insulation.
- Axial dispersion of mass and energy are considered in the gaseous phases.
- Flat profiles of temperature and concentration are assumed along the cross coordinate of each reactor section, based on the selection of sections of narrow height (2 rows of channels).
- Perfectly distributed flux in all channels of the reactor.
- As shown in Fig. 1 (right), two contiguous sections (one of steam reforming and one of combustion) are modeled as representative of the whole reactor. It is assumed that in the same section each channel behaves as the ones in its vicinity.
- Thermal conduction through the metallic walls is considered both axially and transversely.
- Axial thermal conduction through the monolithic catalyst is neglected based on both low cross-sectional area and low conductivity of the ceramic material.
- Homogeneous combustion in fuel mixture section is neglected.

Based on the considerations above, the mathematical model that represents the PPR includes the following equations:

Mass balance in the gas phase

$$\dot{m}_j \cdot \frac{\partial w_{i,j}}{\partial z} = \frac{\partial}{\partial z}\left(\rho_j \cdot D_{i,j} \cdot \frac{\partial w_{i,j}}{\partial z}\right) + k_{g\ i,j} \cdot \rho_j \cdot a_{v,s} \cdot \left(w^s_{i,j} - w_{i,j}\right) \tag{6}$$

Mass balance in the catalyst

$$k_{g\ i,j} \cdot \rho_j \cdot \left(w^s_{i,j} - w_{i,j}\right) = MW_{i,j} \cdot \sum_k \left(\nu_{i,j,k} \cdot r_{j,k}\right) \tag{7}$$

Energy balance in the gas phase

$$\dot{m}_j \cdot \frac{C_{P\,j}}{\overline{MW}_j} \cdot \frac{\partial T_j}{\partial z} = \frac{\partial}{\partial z}\left(\lambda_j \cdot \frac{\partial T_j}{\partial z}\right) + h_j \cdot a_{v,s} \cdot \left(T^s_j - T_j\right) \tag{8}$$

Energy balance in the catalyst

$$(n \cdot a_{v,s}) \cdot h_j \cdot \left(T^s_j - T_j\right) + q_{w\,j} = -(n \cdot a_{v,s}) \cdot \sum_k \left(r_{j,k} \cdot \Delta H_{j,k}\right) \tag{9}$$

Energy balance in the metallic wall

$$\frac{\partial^2 T_w}{\partial z^2} + \frac{\partial^2 T_w}{\partial x^2} = 0 \tag{10}$$

Heat transferred through the metallic wall

$$q_{w\ EC} = a_{v,w} \cdot \lambda_w \cdot \frac{\partial T_w}{\partial x}(\forall z, x = 0) \tag{11}$$

$$q_{w\ ESR} = -a_{v,w} \cdot \lambda_w \cdot \frac{\partial T_w}{\partial x}(\forall z, x = L_X) \tag{12}$$

Boundary conditions

$$z = 0 \rightarrow \begin{cases} \dot{m}_j \cdot \left(w^0_{i,j} - w_{i,j}\right) = -\rho_j \cdot D_{i,j} \cdot \dfrac{\partial w_{i,j}}{\partial z} \\ \dot{m}_j \cdot \dfrac{C_{P\,j}}{\overline{MW}_j} \cdot \left(T^0_j - T_j\right) = -\lambda_j \cdot \dfrac{\partial T_j}{\partial z} \\ \dfrac{\partial T_w}{\partial z} = 0 \quad , \forall x \end{cases} \tag{13}$$

$$z = L_Z \rightarrow \begin{cases} \dfrac{\partial w_{i,j}}{\partial z} = 0 \\ \dfrac{\partial T_j}{\partial z} = 0 \\ \dfrac{\partial T_w}{\partial z} = 0 \quad , \forall x \end{cases} \tag{14}$$

$$\begin{cases} T_w(x = 0) = T^s_{EC.} \\ T_w(x = L_X) = T^s_{ESR.} \end{cases} \quad , \forall z \tag{15}$$

Rate expressions

The reaction rate expressions accounting for the ethanol steam reforming are those reported by López et al. [22]:

$$r_{1,ESR} = k^0_{1,ref} \cdot \exp\left(\frac{-Ea_{1,ESR}}{R \cdot T^s_{ESR}}\right) \cdot \left(p_{EtOH} \cdot p_{H_2O}\right) \tag{16}$$

$$r_{2,ESR} = k^0_{2,ESR} \cdot \exp\left(\frac{-Ea_{2,ESR}}{R \cdot T^s_{ESR}}\right) \cdot \left(p_{CH_4} \cdot p_{H_2O} - \frac{p_{CO} \cdot p^3_{H_2}}{K_{eq,2}}\right) \tag{17}$$

$$r_{3,ESR} = k^0_{3,ESR} \cdot \exp\left(\frac{-Ea_{3,ESR}}{R \cdot T^s_{ESR}}\right) \cdot \left(p_{CO} \cdot p_{H_2O} - \frac{p_{CO_2} \cdot p_{H_2}}{K_{eq,3}}\right) \tag{18}$$

Equilibrium constants, $K_{eq,2}$ and $K_{eq,3}$, are expressed and evaluated by Ref. [28]:

Table 1 – Kinetic parameters for reactions in reforming sections (Eqs. (16)–(18)) [22].

Reaction	$k^0\left[\frac{kmol}{m^2 \cdot s \cdot bar^n}\right]$	$Ea\left[\frac{J}{mol}\right]$
1 (Eq. (1))	$9.40 \cdot 10^5$	148000
2 (Eq. (2))	$8.22 \cdot 10^2$	107300
3 (Eq. (3))	$3.01 \cdot 10^{-1}$	59900

$$\log_{10}(K_{eq,2}) = \frac{-11650}{T^s_{ESR}} + 13.076 \quad (19)$$

$$\log_{10}(K_{eq,3}) = \frac{1910}{T^s_{ESR}} - 1.784 \quad (20)$$

The kinetic parameters corresponding to the ethanol steam reforming rates (Eqs. (16)–(18)) are presented in Table 1.

Regarding ethanol catalytic combustion, the reaction rate expressions (Eqs. (21)–(22)) were those obtained by Bruschi [29] by using the same catalyst adopted previously for ethanol steam reforming by López et al. [22]. Parameters of the combustion rates are reported in Table 2.

$$r_{1,EC} = k^0_{1,EC} \cdot \exp\left(\frac{-Ea_{1,EC}}{R} \cdot \left(\frac{1}{T^s_{EC}} - \frac{1}{T^{ref}_1}\right)\right) \cdot p_{C_2H_5OH} \quad (21)$$

$$r_{2,EC} = k^0_{2,EC} \cdot \exp\left(\frac{-Ea_{2,EC}}{R} \cdot \left(\frac{1}{T^s_{EC}} - \frac{1}{T^{ref}_2}\right)\right) \cdot p_{C_2H_4O} \quad (22)$$

Although these kinetic parameters are fitted by Bruschi [29] at lower temperatures than those T^S explored in this analysis, it is acceptable to consider that the reaction rates are strongly limited by external diffusion due to the elevated temperatures used in this study, as referenced elsewhere [30,31]. Both kinetic models include the mass transfer limitations inside the washcoat.

C_P, μ and λ for single species are expressed according to polynomials as a function of gas temperature [32]. Mixing rules for these properties, and for $D_{i,j}$, are taken from literature [33,34]. As an equation of state, the ideal gas model was selected based on the low pressures and high temperatures at hand. Transport coefficients (h_j, $k_{g\ i,j}$) are obtained from correlations reported elsewhere [15].

Implementation

From the resolution of the system of differential-algebraic equations (Eqs. (6)–(15)) axial temperature and concentration profiles are achieved for the five phases modeled (in fact, a transversal temperature profile is also obtained for the metallic phase). The equation system is solved with gPROMS 3.6™ [35,36]. A central finite differences method was selected to discretize both axial profiles and the transversal coordinate in the metallic wall. The discretized system reaches satisfactory convergence in about 20 s CPU-time in an Intel® Core™ i7-4702MQ computer with 8 GB RAM. To achieve proper convergence of the equation system, resulting variable sets are used in repeated simulations as initial point for the next run. In each iteration, the reaction rate constants are progressively increased from 0 to their actual values.

Table 2 – Kinetic parameters for reactions in combustion sections (Eqs. (21) and (22)) [29].

Reaction	$k^0\left[\frac{mol}{m^2 \cdot s \cdot bar}\right]$	$Ea\left[\frac{J}{mol}\right]$	T^{ref} [K]
1 (Eq. (4))	0.661	169100	598
2 (Eq. (5))	1.233	135900	723

Evaluation of the reactor performance

The reactor performance is evaluated through the distribution of products (molar fractions, $y_{i,j}$), temperature of the gas phases, catalyst phases and metallic wall (T_j, T^s_j and T_w), conversion of ethanol (X_j) and hydrogen yields ($\eta^{ESR}_{H_2}$ and $\eta^{Global}_{H_2}$). These variables are defined as follows:

$$y_{i,j} = \frac{w_{i,j}/MW_{i,j}}{\sum_h (w_{h,j}/MW_{h,j})} \cdot 100 \quad (23)$$

$$X_j = \frac{F^0_{EtOH,j} - F_{EtOH,j}}{F^0_{EtOH,j}} \cdot 100 \quad (24)$$

$$\eta^{ESR}_{H_2} = \frac{F_{H_2,ESR}}{F^0_{EtOH,ESR}} \quad (25)$$

$$\eta^{Global}_{H_2} = \frac{F_{H_2,ESR}}{F^0_{EtOH,ESR} + F^0_{EtOH,EC}} \quad (26)$$

Results and discussion

Base case

A base case of simulation is studied by adopting the parameters reported in Table 3. The specific mass flowrate is selected to achieve a production of hydrogen of 1 kW_{th} (~15 mol_{H_2}/h) at equilibrium conditions at 873.15 K. To these ends, a design comprising 5 sections (both for the reforming and the combustion sides) loaded with monoliths of 2 rows in height and 30 channels in width is selected (i.e., 300 reforming and 300 combustion channels in the whole reactor). Water contents in the reforming feed is selected to meet a steam-to-carbon ratio of 3, the double of the stoichiometric value.

The inlet flowrate and composition of the combustion stream is calculated to provide the reforming channels with

Table 3 – Design parameters and operating conditions, base case of simulation.

Variable	Base case	Variable	Base case
n	2	L_X	0.0012 m
n_S	5	L_Z	0.1500 m
n_R	30	L_W	0.0010 m
T^0_{ESR}	550 °C	T^0_{EC}	550 °C
P_{ESR}	120 kPa	P_{EC}	120 kPa
$\dot{m}_{ESR}$	0.489 kg/(s·m^2)	$\dot{m}_{EC}$	1.931 kg/(s·m^2)
$y^0_{EtOH,ESR}$	14.29%	$y^0_{EtOH,EC}$	0.85%

the necessary heat to achieve the goals specified in the paragraph above. Additionally, an increase in sensible heat of both reforming and combustion streams of +50 K is seeked (i.e., $\Delta T_{outlet\text{-}inlet} = +50$ K). This last constraint assures a ΔT high enough to assure proper operation of the heat exchangers profited outside the reactor to preheat each incoming stream up to the inlet conditions [31].

Hot spots are analyzed, since they must be avoided (or at least minimized), to prevent catalyst deactivation, materials damage, or detachment of the catalytic washcoat due to severe axial temperature gradients. A maximum admisible operating temperature of 770 °C is adopted in order to prevent a reactor material damage and to avoid extrapolation in the range of applicability of the ESR kinetics. In all studied cases, both reforming and combustion streams enter the reactor at the same temperature.

The results of the simulation of the base case are presented in Figs. 2–5. Even when the ethanol conversion in both streams is completed at 2 cm from the entrance (Fig. 2), the products do not achieve completely the chemical equilibrium at the outlet of the unit (Fig. 3). Furthermore, although the aimed hydrogen production is reached in ESR stream (15 mol_{H_2}/h, equivalent to $\eta_{H_2}^{ESR} = 4.35$), the use of ethanol as fuel in the combustion section implies a decrease in the global yield, to a final value of $\eta_{H_2}^{Global} = 3.66$ (Fig. 2).

From the axial temperature profiles presented in Fig. 4, it can be seen that a hot spot reaching 738 °C. This effect is produced due to the fact that combustion reactions have a higher ΔH than steam reforming reactions (Fig. 5). This excess of released energy is gradually consumed by the endothermicity of the ESR reactions, as shown in Fig. 5. The source of heat is in the combustion catalyst, so the temperature of this phase (T_{EC}^{s}) is higher than that of the reforming one (T_{ESR}^{s}), as expected. The reforming gas stream, instead, is heated faster than the combustion gas in the inlet zone (Fig. 4). This is due to a molar flowrate 3-fold larger in the combustion stream implying higher heat capacity and moderating its heating rate. After about 2/3 of the reactor length, the ESR set of reactions shows a light exothermicity based on the water gas shift reaction activity (Eq. (3)). This effect is well balanced by a slight activity in the methane steam reforming (Eq. (2)) which is still

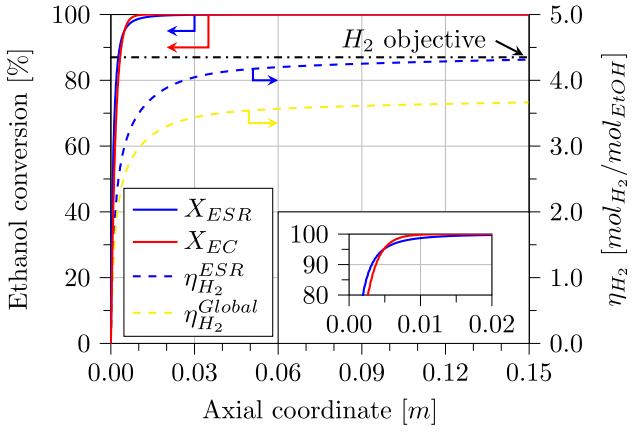

Fig. 2 – Axial profiles of ethanol conversion in both ESR and EC sections and hydrogen yields. Base case of simulation (see Table 3).

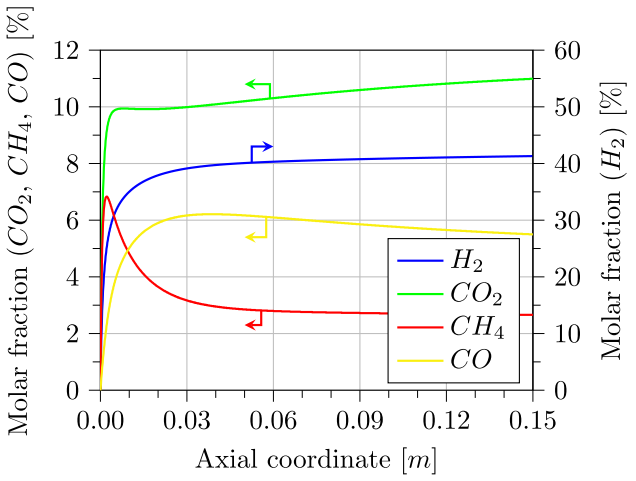

Fig. 3 – Axial molar fraction profiles of the reaction products in the ESR section. Base case of simulation (see Table 3).

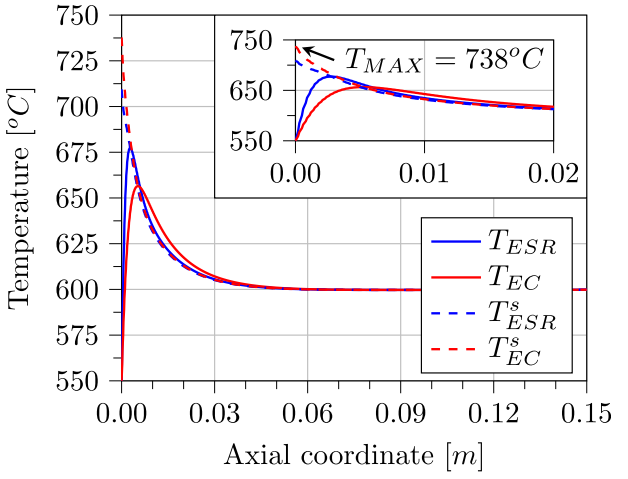

Fig. 4 – Axial temperature profiles (T_w profile is not shown). Base case of simulation (see Table 3).

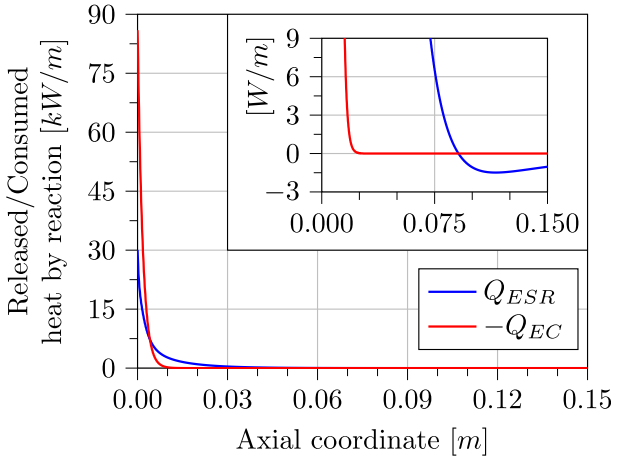

Fig. 5 – Axial profiles of heat generation/consumption rates (negative of combustion values are shown). Base case of simulation (see Table 3).

active, conducting to an isothermic character in the last region of the reactor. Both methane steam reforming (Eq. (2)) and water gas shift reaction (Eq. (3)) still proceed forwards, leading to an increase of hydrogen production, as shown in Fig. 3.

Influence of the thermal level of the reactor

Based on the study of the base case, in this section the impact of the thermal level of the streams on the performance of the reactor is analized. The concentration of ethanol in the combustion stream is selected in each case to achieve a $\Delta T_{outlet\text{-}inlet}$ of +50 K. The ratio of flowrates between the inlet streams of ESR and EC channels is kept constant. Results are reported in Figs. 6 and 7. Fig. 6 shows the outlet molar fractions of CH_4 and CO from the ESR sections, as well as molar fractions of ethanol fed in the EC stream, at different inlet temperatures. For the same conditions, Fig. 7 presents the achieved hydrogen yields and the maximum temperature observed in the reactor for each case.

As shown in Fig. 6, a residual fraction of methane in the ESR stream is observed, even at high temperature, and therefore reaction (2) of the ESR reaction set (Eq. (2)) proceeds forwards. As a consequence, both ESR and global hydrogen yield improve as the inlet temperature is increased (Fig. 7). Special attention has to be put on the molar fraction of CO, which grows as CH_4 is consumed (see Fig. 6), which implies higher volumes for the purification units downstream the reformer, and the level of this species (CO) could be restrictive in the application of this reactor without some purification unit carefully designed.

Moreover, Fig. 6 shows an increasing supply of ethanol as fuel in the EC stream as a higher thermal level is desired. This fact causes a clear separation between the curves of hydrogen yield in the ESR section and global yield (see Fig. 7). Besides, the increase in the ethanol percentage in the EC stream leads to higher reaction rates of combustion. Consequently, higher values of the maximum temperature are seen in Fig. 7. The maximum temperature allowed, imposed at 770 °C, is reached here for an inlet temperature of 585 °C.

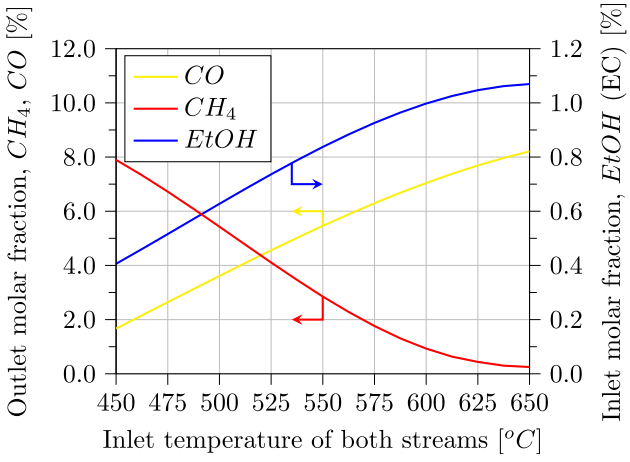

Fig. 6 – Operation at different thermal levels: CO and CH_4 exit molar fractions and required ethanol concentration in the inlet combustion stream. Other design and operation parameters as in Table 3.

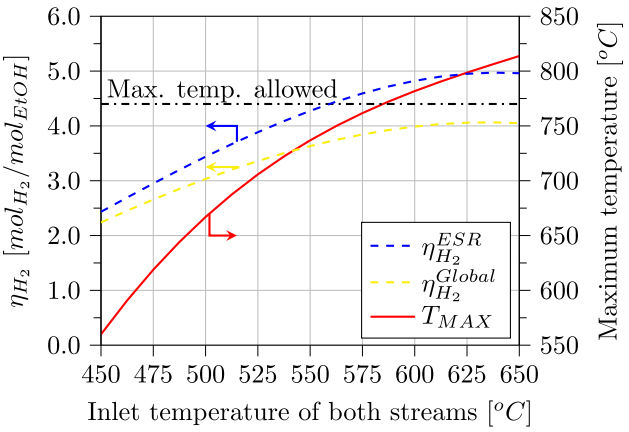

Fig. 7 – Operation at different thermal levels: $\eta_{H_2}^{ESR}$, $\eta_{H_2}^{Global}$ and maximum temperature achieved as a function of the inlet temperature (same for both streams). $y_{EtOH,EC}^0$ as shown in Fig. 6, other design and operation parameters as in Table 3.

Influence of the ethanol combustion flowrate

With the aim of reducing the height of the hot spot near the reactor entrance (e.g., in the base case, reaching almost 740 °C), the heat capacity of the EC stream can be enhanced by increasing the combustion stream flowrate. In order to keep delivering the same quantity of heat to the ESR reaction, the total molar flux of ethanol in the EC stream is kept constant. This restriction leads to a drop in the concentration of ethanol fuel, as shown in Fig. 8. The correspondent maximum temperatures observed inside the unit are shown in Fig. 9.

Clearly, this option satisfies the achievement of a lower hot spot, but the necessary flowrate could be high enough to lead to restrictive pressure drops on the combustion side. Alternatively, the next sections expose the study of different design

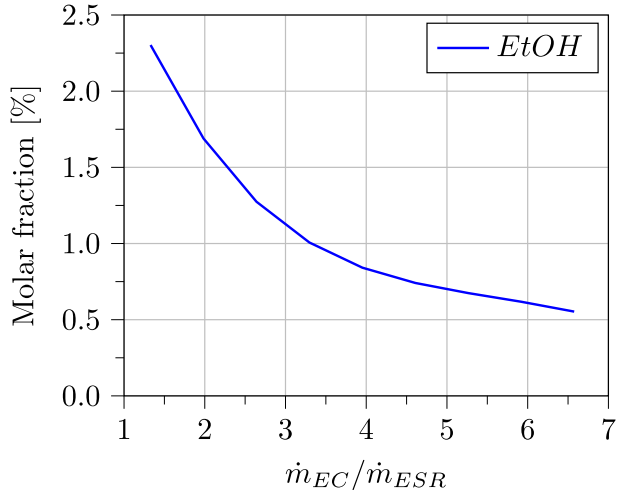

Fig. 8 – Influence of the combustion total flowrate (constant reforming flowrate): required ethanol concentration in the combustion inlet. Other design and operation parameters as in Table 3.

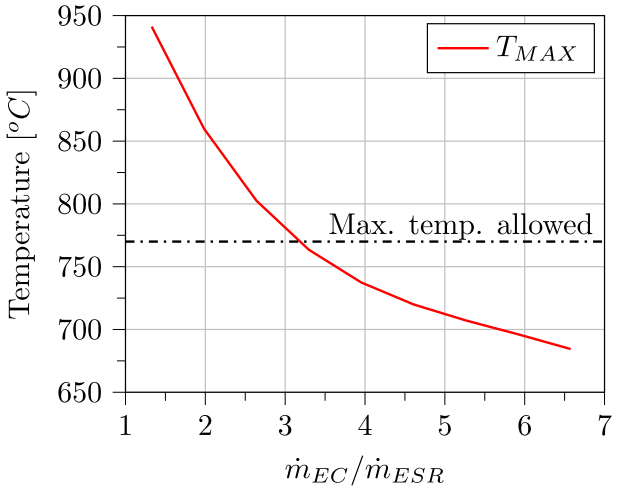

Fig. 9 – Influence of the combustion total flowrate (constant reforming flowrate): maximum temperature achieved. Ethanol concentration as shown in Fig. 8; other design and operation parameters as in Table 3.

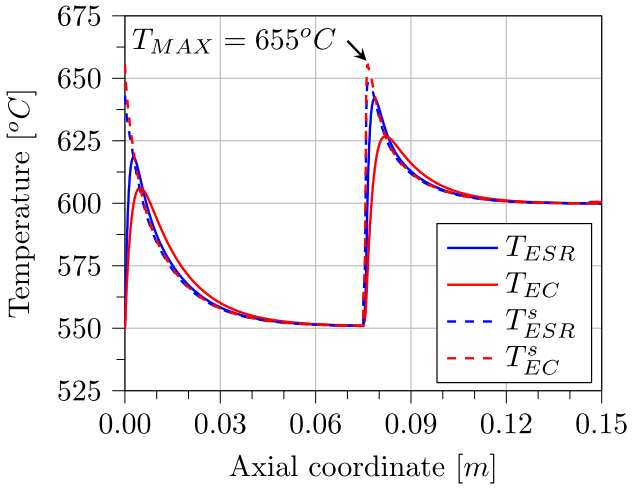

Fig. 10 – Axial temperature profiles for a reactor design with one lateral fuel injection port in the combustion section and using the same amount of total ethanol fuel as in the base case (50% to each inlet); other design and operation parameters as in Table 3.

options including the redistribution of the ethanol fuel in more than one injection port.

Design with axial distribution of the ethanol fuel

Case 1: Constant total amount of fuel

As seen in the previous subsections, elevated temperatures (some of them prohibitive values) are reached at the hot spots occurring near the reactor entrance. The approach to the equilibrium presented by the ESR system limits the possibility of improving the performance of the reactor. This fact cannot be solved easily through the variation of the thermal level since the operation temperature is close enough to the maximum allowed. As an alternative, the distribution of the total fuel in two or three ports along the axial coordinate of the reactor is proposed. Here, a portion of the ethanol to be combustioned is added at the entrance of the reactor together with the total flowrate of air. The temperature of the lateral ethanol stream is set to T^0_{EC} in order to make negligible any cold-shot effect in the reactor. Then, by using one or two lateral injections, the remaining ethanol is added to promote a new source of heat to be transferred to the reforming channels. The axial position of the lateral ports considers leaving equal amounts of catalysts in each axial zone between ports.

In this case study, the total quantity of fuel is the same as in the base case (see Table 3), but as shown in Figs. 10 and 11, the maximum temperature in the reactor decreases considerably. In fact, a maximum temperature of 655 °C is observed for a design with a single lateral injection port. When two lateral injection ports are used (Fig. 11), the maximum temperature is 636 °C. In both cases, the outlet temperature of the streams (600 °C) is about 50 °C higher than the entrance temperature, fulfilling the $\Delta T_{outlet\text{-}inlet}$ objective.

Figs. 12 and 13 complete the analysis of this case study; for the sake of comparison, results of the base case have been included as well. Results show that while the shape of the thermal profiles have changed (compare Figs. 10 and 11 with

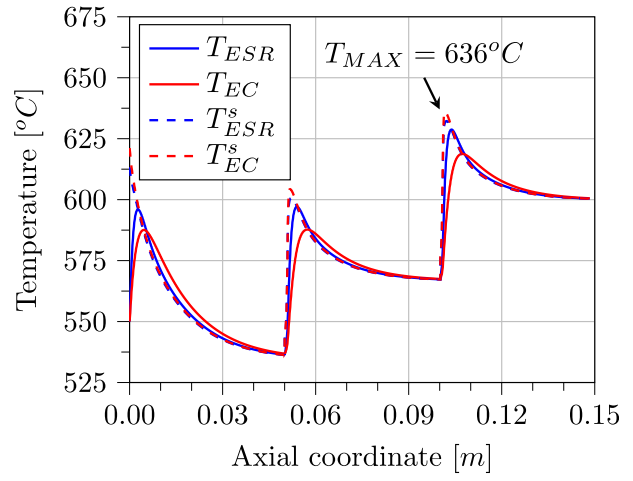

Fig. 11 – Axial temperature profiles for a reactor design with two lateral fuel injection port in the combustion section and using the same amount of total ethanol fuel as in the base case (33.3% in each inlet); other design and operation parameters as in Table 3.

Fig. 4), the reactor has the proper length to obtain the same outlet distribution of products, and ESR and global hydrogen yields. This is a good result since, in this way, the thermal level could be diminished, maintaining the aimed levels of quality in the products. Furthermore, and moving a step forward, a distributed fuel design can be combined with extra fuel addition to catch the advantages of operating the reactor at a higher mean thermal level without surpassing the maximum allowable temperature. These results are discussed in the following paragraphs.

Case 2: Hot spots of equal height

This section describes the results of distributing the ethanol fuel in more than one inlet, considering as a constraint the

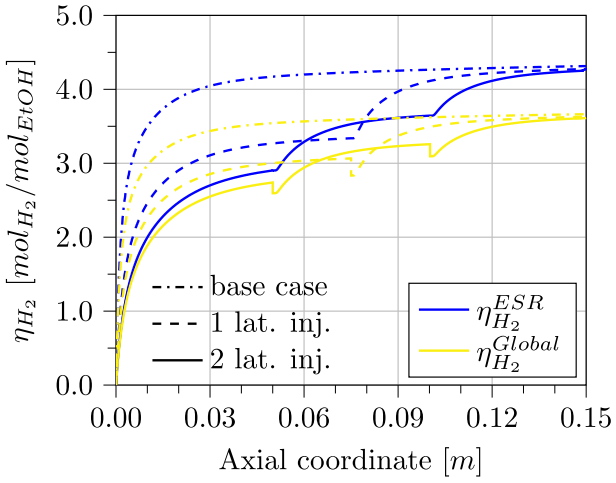

Fig. 12 – Axial profiles of $\eta_{H_2}^{ESR}$ and $\eta_{H_2}^{Global}$ for the operation in the base case and with the designs with one and two lateral fuel injection ports. The same total amount of fuel is adopted (as in Table 3).

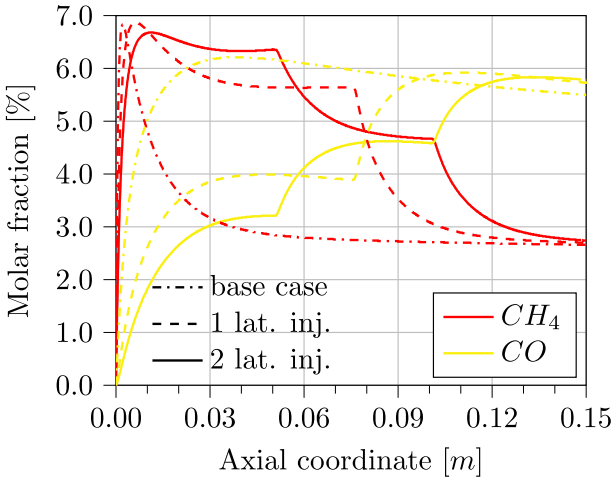

Fig. 13 – Axial profiles of $y_{CH_4,ESR}$ and $y_{CO,ESR}$ for the base case and with the designs with one and two lateral fuel injection ports. The same total amount of fuel is adopted (as in Table 3).

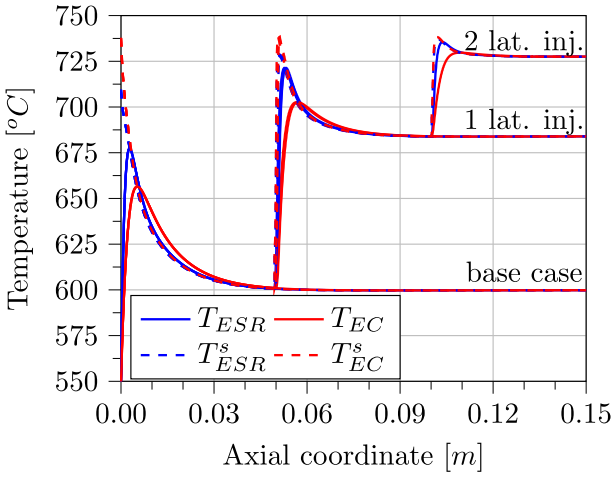

Fig. 14 – Axial temperature profiles for the operation in the base case and with the designs with one and two lateral fuel injection ports and achieving the same maximum temperature as in the base case of simulation; other design and operation parameters as in Table 3.

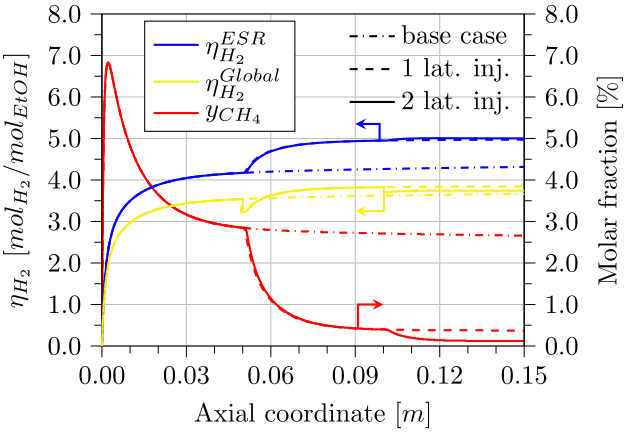

Fig. 15 – Axial profiles of $y_{CH_4,ESR}$, $\eta_{H_2}^{ESR}$ and $\eta_{H_2}^{Global}$ for the base case and with the designs with one and two lateral fuel injection ports, achieving the same maximum temperature as in the base case of simulation; other design and operation parameters as in Table 3.

addition of ethanol such as to achieve the same maximum temperature in the each hot spot as in the base case (738 °C). Results are presented in Figs. 14 and 15.

Fig. 14 shows a comparison of the temperature profiles of the base case with those designs with one or two lateral injections. To obtain the same maximum temperature at the three reactor zones, the first lateral injection adds a quantity equivalent to 65% of the ethanol at the entrance, while the second port adds an extra 25%. In this case (2 lateral injections), the total quantity of ethanol in the EC stream is 190% of the base case. The $\Delta T_{outlet\text{-}inlet}$ using only the first lateral injection reaches 135 °C, while with the inclusion of the second lateral injection the value rises up to 177 °C. The cost of the fuel in excess would be partially compensated with smaller external heat exchangers due to the higher ΔT available for the preheating of both feed streams (i.e., reforming and combustion sides). Nevertheless, a deeper analysis of the complete periphery seems mandatory.

Axial profiles of methane molar fraction and ESR and global hydrogen yields are presented in Fig. 15. While the concentration of methane at the reactor outlet decreases with the addition of extra fuel via the lateral injection ports, the outlet hydrogen yield in the ESR stream increases as a result of extra steam reforming of methane. The ESR hydrogen yield presents a pronounced increment after the first lateral injection with respect to the base case ($\eta_{H_2}^{ESR} = 4.32 \rightarrow 4.97$), and an almost insignificant increase after the second lateral port with respect to the first one ($\eta_{H_2}^{ESR} = 4.97 \rightarrow 5.00$). Furthermore, the second lateral injection has a negative impact in the global

yield ($\eta_{H_2}^{Global} = 3.74$) as it drops with respect to the design with only one lateral injection ($\eta_{H_2}^{Global} = 3.85$).

Summing up, the use of a single lateral injection port appears to be the best alternative providing enhanced reactor performance and preventing the increase in manufacture complexity related with multiple lateral injections.

Conclusions

This paper reports the results of the mathematical simulation resembling the performance of a Parallel Plates Reactor (PPR) for the autothermal generation of hydrogen from ethanol. Structured catalysts are used inside the reactor to conduct both ethanol steam reforming and ethanol combustion with air. Thermal coupling between combustion and reforming of ethanol is plausible and an adequate behavior of the reactor in terms of hydrogen yield and conversion of ethanol is predicted. For the objective of a production of hydrogen equivalent to 1 kW_{th} (~15 mol_{H_2}/h) a reactor comprising 300 channels of 1 mm^2 for ESR and 300 channels for EC, and a 15 cm of reactor length is suggested. A restriction of +50 K was imposed to the $\Delta T_{outlet\text{-}inlet}$ to assure the operability of external heat exchangers required outside the unit to preheat each stream with itself up to the inlet conditions. The base case presents a maximum temperature in the entrance region of the reactor of 738 °C, 188 °C over the level of the inlet streams (550 °C).

The importance of the pre-heating level of the streams before entering the reactor is evidenced in terms of hydrogen yields. While for the base case the global hydrogen yield is 4.35 mol_{H_2}/mol_{EtOH}, an inlet temperature of 450 °C could lead to a value of 2.5 mol_{H_2}/mol_{EtOH}. Inlet temperatures over 585 °C result in maximum temperature values over the restriction imposed at 770 °C and should be avoided for this design. High molar fractions of ethanol in the combustion stream can lead to excessive hot spots if they are not adequately balanced by adjusting the total flowrate of the combustion stream. Nevertheless, total flowrates on the combustion side cannot be increased arbitrarily as prohibitive pressure drops posses a restriction. To satisfy the constraint of not surpassing the maximum temperature allowed, and to accomplish simultaneously the objective of hydrogen production, design alternatives including single or multiple lateral injection ports for the ethanol in the combustion channels were studied.

Aiming to fulfill the desired production of hydrogen, a satisfactory option when compared with the fuel injection at the reactor mouth seems to be the distribution of the fuel, using lateral injections. This design reduces significantly the observed hot spots (about 100 °C) while retaining the rest of the reactor performance. On the other hand, if increasing the thermal level of the reactor without surpassing a maximum temperature is desired, the distributed fuel injection allows increasing the hydrogen yield by permitting more ethanol fuel being burned. In this case, the use of a single lateral port (in addition to the reactor mouth) is preferred; extra lateral ports increase the manufacture complexity without enhancing the hydrogen yield or even decreasing it.

Nomenclature

Compounds and Sections		
i	Compounds of each section j.	
	Sections of the reactor:	
	1: Ethanol Steam Reforming (ESR)	
j	2: Ethanol Combustion (EC)	
k	Reactions in each section j.	
$j = 1$	i_1: Ethanol (EtOH)	
	i_2: Water (H_2O)	
	i_3: Hydrogen (H_2)	
	i_4: Carbon Dioxyde (CO_2)	
	i_5: Methane (CH_4)	
	i_6: Carbon Monoxyde (CO)	
	k_1: $C_2H_5OH + H_2O \rightarrow CH_4 + CO_2 + 2H_2$ (Eq. (1))	
	k_2: $CH_4 + H_2O \leftrightarrow CO + 3\,H_2$ (Eq. (2))	
	k_3: $CO + H_2O \leftrightarrow CO_2 + H_2$ (Eq. (3))	
$j = 2$	i_1: Ethanol (EtOH)	
	i_2: Oxygen (O_2)	
	i_3: Nitrogen (N_2)	
	i_4: Carbon Dioxyde (CO_2)	
	i_5: Water (H_2O)	
	i_6: Acetaldehyde (C_2H_4O)	
	k_1: $C_2H_5OH + 1/2O_2 \rightarrow C_2H_4O + H_2O$ (Eq. (4))	
	k_2: $C_2H_4O + 5/2O_2 \rightarrow 2CO_2 + 2H_2O$ (Eq. (5))	
Variables of the Mathematical Model		
$a_{v,s}$	Specific area of the catalytic channels.	m^2/m^3
$a_{v,w}$	Specific area of heat transfer through the metalic wall.	m^2/m^3
$C_{P\,j}$	Heat capacity of the mixture in section j.	$J/(mol\ °C)$

$D_{i,j}$	Diffusion coefficient of the ith species in the gas phase, in section j.	m^2/s
$F_{i,j}$	Specific molar flowrate of the ith species in the gas phase, in section j.	$mol/(m^2\ s)$
h_j	Heat transfer coefficient in section j.	$W/(m^2\ ^\circ C)$
ΔH^0	Standard heat of reaction.	kJ/mol
$\Delta H_{j,k}$	Heat of the reaction k, in section j.	J/mol
$k_{g\ i,j}$	Mass transfer coefficient of the ith species, in section j.	m/s
$k^0_{k,j}$	Arrhenius constant of the reaction k of the section j, see units in Tables 1 and 2.	
$K_{eq,2/3}$	Equilibrium constants for the ESR section.	
L_W	Width of the catalytic channel.	M
L_X	Thickness of the metallic wall.	M
L_Z	Length of the reactor.	M
$\dot{m}_j$	Specific mass flowrate in section j.	$kg/(m^2\ s)$
$MW_{i,j}$	Molecular weight of the ith species, in section j.	kg/mol
$\overline{MW}_j$	Average molecular weight of the mixture in section j.	kg/mol
n	Number of channels per row of monolith in one section of reaction in each side.	
n_R	Number of rows of monolith in one section of reaction in each side.	
n_S	Number of sections of reaction in each side.	
$p_{i,j}$	Partial pressure of the ith species, in the catalytic section j.	Bar
P_j	Pressure in section j.	kPa
$q_{w\ j}$	Heat transferred through the metallic wall, from/to section j.	W/m^3
Q_j	Consumed/Released heat by reactions in section j.	kW/m
R	Universal gas constant.	$J/(mol\cdot^\circ C)$
$r_{j,k}$	Rate of the reaction k, in section j.	$mol/(m^2\ s)$
T_j	Temperature of the gas phase, in section j.	$^\circ C$
T^s_j	Temperature of the catalytic phase, in section j.	$^\circ C$
T_w	Temperature of the metallic wall.	$^\circ C$
T^0_j	Temperature at the entrance of the reactor, in section j.	$^\circ C$
$w_{i,j}$	Mass fraction of the ith species in the gas phase, in section j.	
$w^s_{i,j}$	Mass fraction of the ith species in the catalytic phase, in section j.	
x	Transversal coordinate of the metallic wall.	M
X_j	Ethanol conversion in section j.	%
$y_{i,j}$	Molar fraction of the ith species in the gas phase, in section j.	%
z	Axial coordinate of the reactor.	M
$\eta^{ESR}_{H_2}$	Hydrogen yield in ESR section.	mol_{H_2}/mol_{EtOH}
$\eta^{Global}_{H_2}$	Global hydrogen yield.	mol_{H_2}/mol_{EtOH}
λ_w	Thermal conductivity of the metallic wall.	$W/(m\ ^\circ C)$
λ_j	Thermal conductivity of the mixture in section j.	$W/(m\ ^\circ C)$
μ_j	Viscosity of the mixture in section j.	$Pa\cdot s$
$\nu_{i,j,k}$	Stoichiometric coefficient of the ith species, in section j, for the reaction k.	
ρ_j	Density of the gas phase in section j.	kg/m^3

Acknowledgements

The authors acknowledge the financial support of Consejo Nacional de Investigaciones Científicas y Técnicas (CONICET), Universidad Nacional del Sur (UNS), and Agencia Nacional de Promoción Científica y Tecnológica (ANPCyT).

REFERENCES

[1] Das D, Veziroğlu TN. Hydrogen production by biological processes: a survey of literature. Int J Hydrogen Energy 2001;26(1):13–28.
[2] Dodds PE, Staffell I, Hawkes AD, Li F, Grünewald P, McDowall W, et al. Hydrogen and fuel cell technologies for heating: a review. Int J Hydrogen Energy 2015;40(5):2065–83.
[3] Kim T. Micro methanol reformer combined with a catalytic combustor for a PEM fuel cell. Int J Hydrogen Energy 2009;34:6790–8.
[4] Gardemann U, Steffen M, Heinzel A. Design and demonstration of an ethanol fuel processor for HT-PEM fuel cell applications. Int J Hydrogen Energy 2014;39(31):18135–45.
[5] Ni M, Leung DYC, Leung MKH. A review on reforming bio-ethanol for hydrogen production. Int J Hydrogen Energy 2007;32:3238–47.
[6] Hernández L, Kafarov V. Use of bioethanol for sustainable electrical energy production. Int J Hydrogen Energy 2009;34(16):7041–50.
[7] Vaidya PD, Rodrigues AE. Insight into steam reforming of ethanol to produce hydrogen for fuel cells. Chem Eng J 2006;117:39–49.
[8] Haryanto A, Fernando SD, Murali N, Adhikari S. Current status of hydrogen production techniques by steam reforming of ethanol: a review. Energy Fuels 2005;19(11):2098–106.
[9] Hou T, Zhang S, Chen Y, Wang D, Cai W. Hydrogen production from ethanol reforming: catalysts and reaction mechanism. Renew Sustain Energy Rev 2015;44:132–48.
[10] Contreras JL, Salmones J, Colín-Luna JA, Nuño L, Quintana B, Córdova I, et al. Catalysts for H2 production using the ethanol steam reforming (a review). Int J Hydrogen Energy 2014;39(33):18835–53.
[11] Mas V, Kipreos R, Amadeo NE, Laborde MA. Thermodynamic analysis of ethanol/water system with the stoichiometric method. Int J Hydrogen Energy 2006;31:21–8.
[12] Graschinsky C, Giunta P, Amadeo N, Laborde MA. Thermodynamic analysis of hydrogen production by autothermal reforming of ethanol. Int J Hydrogen Energy 2012;7:10118–24.
[13] Baruah R, Dixit M, Basarkar P, Parikh D, Bhargav A. Advances in ethanol autothermal reforming. Renew Sustain Energy Rev 2015;51:1345–53.
[14] Frauhammer J, Eigenberger G, Hippel LV, Arntz D. A new reactor concept for endothermic high-temperature reactions. Chem Eng Sci 1999;54:3661–70.
[15] Cybulski A, Moulijn JA. Monoliths in heterogeneous catalysis. Catal Rev 1994;36(2):179–270.
[16] Saber M, Commenge JM, Falk L. Microreactor numbering-up in multi-scale networks for industrial-scale applications: impact of flow maldistribution on the reactor performances. Chem Eng Sci 2010;65(1):372–9.
[17] Rahimpour MR, Dehnavi MR, Allahgholipour F, Iranshahi D, Jokar SM. Assessment and comparison of different catalytic coupling exothermic and endothermic reactions: a review. Appl Energy 2012;99:496–512.
[18] Kolios G, Frauhammer J, Eigenberger G. Efficient reactor concepts for coupling of endothermic and exothermic reactions. Chem Eng Sci 2002;57:1505–10.
[19] Kolios G, Gritsch A, Morillo A, Tuttlies U, Bernnat J, Opferkuch F, et al. Heat-integrated reactor concepts for catalytic reforming and automotive exhaust purification. Appl Catal B Environ 2007;70:16–30.
[20] Zanfir M, Gavriilidis A. Modelling of a catalytic plate reactor for dehydrogenation-combustion coupling. Chem Eng Sci 2001;56:2671–83.
[21] Zanfir M, Gavriilidis A. Catalytic combustion assisted methane steam reforming in a catalytic plate reactor. Chem Eng Sci 2003;58:3947–60.
[22] López E, Gepert V, Gritsch A, Nieken U, Eigenberger G. Ethanol steam reforming thermally coupled with fuel combustion in a parallel plate reactor. Ind Eng Chem Res 2012;51:4143–51.
[23] Casanovas A, Saint-Gerons M, Griffon F, Llorca J. Autothermal generation of hydrogen from ethanol in a microreactor. Int J Hydrogen Energy 2008;33:1827–33.
[24] Bruschi YM, López E, Schbib NS, Pedernera MN, Borio DO. Theoretical study of the ethanol steam reforming in a parallel channel reactor. Int J Hydrogen Energy 2012;37:14887–94.
[25] Bruschi YM, López E, Pedernera MN, Borio DO. Coupling exothermic and endothermic reactions in an ethanol microreformer for H2 production. Chem Eng J 2016;294:97–104.
[26] Peluso MA, Pronsato E, Sambeth JE, Thomas HJ, Busca G. Catalytic combustion of ethanol on pure and alumina supported K-Mn oxides: an IR and flow reactor study. Appl Catal B Environ 2008;78:73–9.
[27] Campesi MA, Mariani NJ, Bressa SP, Pramparo MC, Barbero BP, Cadús LE, et al. Kinetic study of the combustion of ethanol and ethyl acetate mixtures over a MnCu catalyst. Fuel Process Technol 2012;103:84–90.
[28] De Groote A, Froment GF. Reactor modeling and simulations in synthesis gas production. Rev Chem Eng 1995;11(2):145–83.
[29] Bruschi YM. Estudio de micro-reactores para la generación de gas de síntesis. Bahía Blanca: Ph.D. Thesis. Argentina: Universidad Nacional del Sur; 2014. http://repositoriodigital.uns.edu.ar/handle/123456789/437.
[30] Morillo A, Freund A, Merten C. Concept and design of a novel compact reactor for autothermal steam reforming with integrated evaporation and CO cleanup. Ind Eng Chem Res 2004;43(2):4624–34.
[31] Gritsch A. Wärmeintegrierte Reaktorkonzepte für katalytische Hochtemperatur-Synthesen am Beispiel der dezentralen Dampfreformierung von Methan. Sttutgart: Ph.D. Thesis. Germany: Universität Stuttgart; 2008. https://elib.uni-stuttgart.de/handle/11682/1788.
[32] Yaws C. Chemical properties handbook. New York: McGraw-Hill; 1999.
[33] Wilke CR. A viscosity equation for gas mixtures. J Chem Phys 1950;18(4):517–9.
[34] Poling BE, Prausnitz JM, O'connell JP. The properties of gases and liquids. New York: McGraw-Hill; 2001.
[35] Oh M, Pantelides CC. A modelling and simulation language for combined lumped and distributed parameter systems. Comput Chem Eng 1996;20(6–7):611–33.
[36] PSE. gPROMS introductory user guide. London: Process Systems Enterprise Ltd.; 2004.